

Experimental search for one-dimensional edge states at surface steps of the topological insulator Bi_2Se_3 : distinguishing between effects and artifacts

N.I. Fedotov and S.V. Zaitsev-Zotov

Kotel'nikov Institute of Radioengineering and Electronics of RAS, Mokhovaya 11, bld. 7, Moscow, 121069 Russia

(Dated: September 29, 2016)

Results of detailed study of the topological insulator Bi_2Se_3 surface state energy structure in the vicinity of surface steps by scanning tunneling microscopy (STM) and spectroscopy (STS) methods are presented. Growth of the chemical potential level in the vicinity of the step edge is observed. The value of the growth is found to correlate with the step height and is caused by redistribution of electron wave functions between outer and inner edges of surface steps, as it is known for usual metals. Smaller value of the shift and its larger characteristic length reflect specifics of the helical surface states. This growth is accompanied by increase of the differential tunneling conductance, dI/dV , in the helical surface states energy region and thereby produces illusion of appearance of the edge states. We show that this growth is reproduced in the framework of the tunneling model paying attention to taking into account the tunneling gap transparency change.

INTRODUCTION

Termination of periodic potential of a crystal by a surface results in appearance of surface states known as Tamm [1] or Shokley [2] states. The states are degenerate by spin, localized near the surface and decay exponentially in the direction perpendicular to the surface. Recent classification of crystalline solids by topological invariant reveals another type of surface states whose existence is protected by time-reversal symmetry [3]. These gapless helical Dirac fermion states have a specific cone-like spectrum (so-called Dirac cone) crossing the entire bulk energy gap, they are degenerate (except for the cone apex called Dirac point) and characterized by the spin-momentum locking, the spin being orthogonal to the momentum. In particular, three-dimensional topological insulators (TI) Bi_2Te_3 and Bi_2Se_3 host a single Dirac cone with the Dirac point at Γ point of the Brillouin zone [4].

The crystal surface is also a periodic object and a question arises what happens with the surface states if this periodicity is also terminated, for instance, by the crystal face at a surface step? In the case of topologically trivial material with conducting surface states the answer is well known: an interference pattern appears due to interference of incident and scattered states [5]. The answer for topologically nontrivial insulators is still not well known. If the bulk state of an insulator is characterized by nonzero topological invariant Z_2 , then the existence of the surface states is protected by the time-reversal symmetry and the momentum of the surface electrons is locked to their spin. As a change of momentum direction means now spin direction change, this circumstance destroys interference and new features are expected to appear.

Scanning tunneling microscopy (STM) and spectroscopy (STS) provide the most direct information on local properties in the vicinity of various surface defects. Experimental studies of the effect of surface steps on surface electronic states in TI by these methods reveal a

number of new features. First of all, standard interference patterns formed around the steps are observed for electronic states far from the Dirac point $k \gtrsim 0.1 \text{ \AA}^{-1}$ both in Bi_2Te_3 [6, 7] and Bi_2Se_3 [8]. The interference pattern amplitude vanishes upon approaching the bulk energy gap edge from bulk band states side, so no interference is seen for pure helical states [7].

Electron states which may appear at the edge between two adjacent TI crystal surfaces hosting helical states (or surfaces with different velocities of massless Dirac fermions) were also studied theoretically [9–15]. Edge states were predicted to appear along the edge between two surfaces [10, 14] or at the sides of a strip [12] of a three-dimensional topological insulator such as Bi_2Se_3 , but to the best of our knowledge, were not yet reported experimentally for this material. In the topological insulator Bi_2Te_3 a bound state along a step on the surface was found to appear [7]. Namely, the local density of states increases by a few tens percents within 1–2 nm near the step edge forming thereby a sort of an edge state [7]. Energy dispersion of such states and their existence in other materials such as Bi_2Se_3 are still open questions.

Here we present the results of detailed study of Bi_2Se_3 energy structure in the vicinity of surface steps by STS methods. We observed a smooth variation of the chemical potential level by 0.1–0.2 eV, the screening length ($\sim 10 \text{ nm}$) being practically independent of the carrier concentration. In addition, a growth of the differential tunneling conduction, dI/dV , in the vicinity of the steps is observed and produce an illusion of the edge states. We show here that this growth can be practically entirely accounted if the bias-induced change of transparency of the tunneling gap is taken into account.

EXPERIMENTAL AND METHODOLOGICAL NOTES

Bi_2Se_3 crystals were grown from a mixture of Bi and Se with a 3% excess of Se over stoichiometric quantity

by heating followed by smooth cooling down in evacuated quartz ampules, growth details are available elsewhere [16]. The experiments have been carried out with “standard” n -type Bi_2Se_3 crystals (group I), as well as on Bi_2Se_3 crystals with the chemical potential position inside the bulk band gap (group II). STM and STS measurements were performed with an Omicron LT-STM operating at a base pressure of 2×10^{-11} Torr. The samples were exfoliated *in situ* at room temperature and transferred to the low-temperature section of the STM kept at liquid helium temperature. Tips cut from Pt-Rh wire were used for imaging and spectroscopy. The quality of tips was checked on Au foil before and after the measurements by checking the linearity of the I - V characteristic in the vicinity of $V=0$. If needed we performed a tip recovery procedure which includes a short dipping the tip into the Au surface followed by the standard tip control procedure described above. The STM images were recorded in the constant current mode. I - V curves were acquired in the spectroscopy mode and numerically differentiated. The results discussed below represent a typical behavior observed in 2 group I samples (6 steps) and 7 group II samples (14 steps). Some preliminary results obtained for group II samples can be found in Ref. [16]

Structurally Bi_2Se_3 consists of quintuple layers (QL) Se-Bi-Se-Bi-Se, stacked on top of each other and bound together by Van der Waals force, so the crystals are easily cleaved between the layers and steps on the Bi_2Se_3 usually correspond to an integer number of QLs.

Regions of the sample surface containing steps and other extended defects were selected for the study. Typical STM images of such regions are presented in Fig. 1. Terraces separated by one (Fig. 1(a)) or two steps (Fig. 1(b)) are clearly seen. Step height corresponds to one or two quintuple layers. Inset in Fig. 1(a) shows a fragment of the surface with atomic resolution. We see that the step edge orientation mostly consists of $[\bar{2}110]$ segments connected by relatively short $[\bar{1}100]$ ones.

A typical differential tunneling conductance curve obtained away from defects is shown in Fig. 2(a). The Dirac point of Bi_2Se_3 is in the bulk band gap and is identified as the minimum of the V-shaped feature. Identification of the bulk valence and conduction band positions is based on assumption of the bulk energy gap value 0.3 eV [6]. The spectra we observed on group II samples (Fig. 2(b)) are somewhat different: their minima are ≈ 80 meV closer to the conduction band and have lower differential conductance value. This may be due to a different Dirac point position with respect of bulk bands in group II samples, or a dip in differential tunneling conductance around E_F , masking the true position of V_D . The chemical potential level of group I samples is near the bottom of the bulk conduction band providing n -type conduction, (Fig. 2(a)), whereas it is within ± 50 meV from the Dirac point in group II samples (Fig. 2(b)).

When exploring the spatial variation of scanning tun-

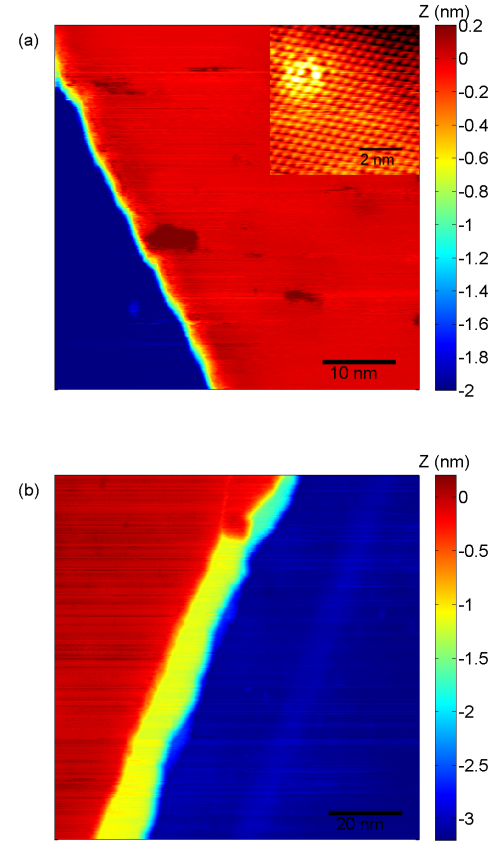


FIG. 1: STM images of Bi_2Se_3 surfaces with steps of different heights: type (I) sample with 2QL high step, inset shows the atomic resolution image; type(II) sample with 1QL and 2QL steps. In both cases $V_t = -0.4$ V, $I_t = 100$ pA, $T = 5$ K.

neling spectra one needs to take into account the fact that they strongly depend on tip-sample separation, which is different in different points of the sample surface due to the feedback maintaining the tunneling current at a certain set voltage. So a proper choice of LDOS data normalization is required to compare the data obtained at different levels of the chemical potential. In the simplest case the effect of changing tip-sample distance amounts to a multiplication by an exponential factor. To take this factor into account we normalize the differential conductance curve by its value at a specific energy. Since a shift of the chemical potential occurs, this voltage cannot be fixed but needs to be tied to the energy structure of the sample.

First of all we assume that the bulk energy structure (namely, valence and conduction bands separation) does not change near the step. If so, they can be used as a reference for determination of the chemical potential level position with respect to the bulk bands. We assume that the bulk states are only shifted as a whole. To measure such a shift, we select a certain value of ΔV ,

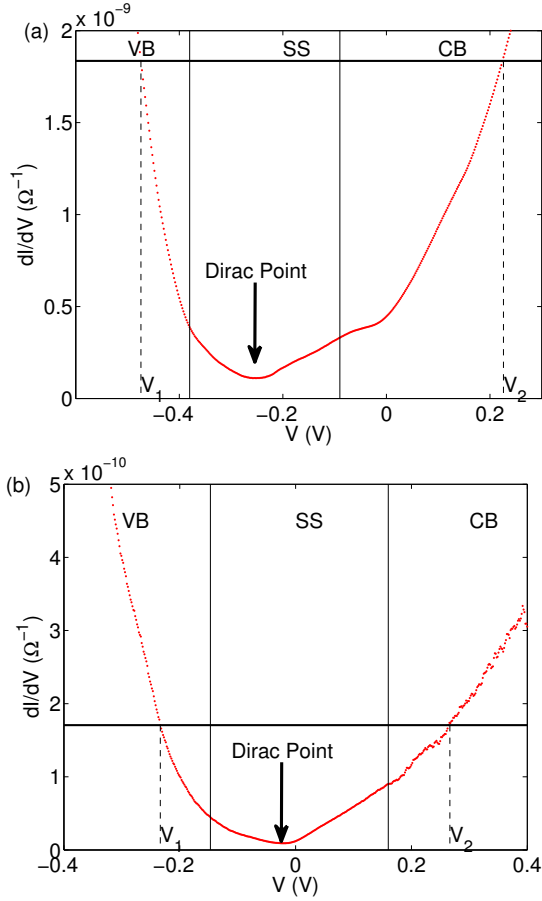


FIG. 2: Typical differential conductance curve of Bi_2Se_3 surface away from defects (group II sample). Bulk valence band (VB), bulk conduction band (CB) and surface states (surface states), are separated by vertical lines. The arrow points to the Dirac point identified as the minimum of the differential conductance curve. V_1 and V_2 corresponds to $\Delta V = 0.7$ V for group I samples (a) and 0.5 V for group II samples (b) (see text for details). Set point $V_t = -0.4$ V, $I_t = 100$ pA, $T = 5$ K.

which is bigger than the bulk energy gap and find two points V_1 and V_2 at which the energy width of the differential conductance curve equals to ΔV (see Fig. 2), so that $V_2 - V_1 = \Delta V$, and $\frac{dI}{dV}|_{V_1} = \frac{dI}{dV}|_{V_2} = G_t$. We normalize our curves by the value of the tunneling differential conductance, G_t , at these points. We find that such a choice of normalization makes dI/dV curves of very different samples measured at different set points to be very similar.

V_1 allows us to trace the shift of the bulk bands. Assuming that $V_D - V_1 = \text{const}$ we can trace V_D position (or the chemical potential position) over entire sample surface despite the fact that defects may modify LDOS near V_D significantly. As the Dirac point may be actually absent at certain defects, we will use the $V_0 = V_1 + \alpha \Delta V$ as a notation for suggested V_D position, where α is chosen to provide $V_0 = V_D$ far from defects. For group I samples

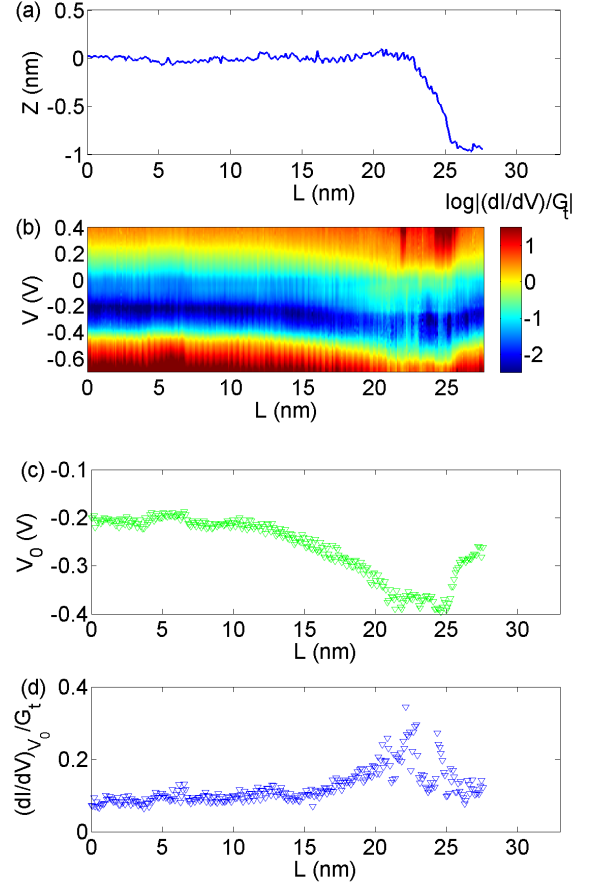


FIG. 3: Profile along a scan line crossing a QL step on Bi_2Se_3 (group I) surface (upper curve) and respective set of dI/dV curves (middle, pay attention to the logarithmic color scale) and the Dirac point position along the scan line (bottom). I - V curves were collected at $V_t = -0.4$ V, $I_t = 100$ pA, $T = 5$ K.

we choose $\Delta V = 0.7$ eV, $\alpha = 0.34$ and for group II samples $\Delta V = 0.5$ eV, $\alpha = 0.32$ since the voltage range in group II measurements is not wide enough for $\Delta V = 0.7$ eV.

RESULTS

STS results along a line. Shift of the chemical potential level

We performed two types of STS measurements. The first one provides a set of I - V curves taken along a line crossing the step. Typical results obtained for groups I and II samples are shown in Fig. 3,4.

Let us analyze Fig. 3 in more details. The step edge is at $L \approx 22$ nm, the step height corresponds to 1QL. A small bump near the step edge is caused by growth of the LDOS at the set point ($V_t = -0.4$ V), as seen from Fig. 3(b). The step edge profile (Fig. 3(a)) looks smooth

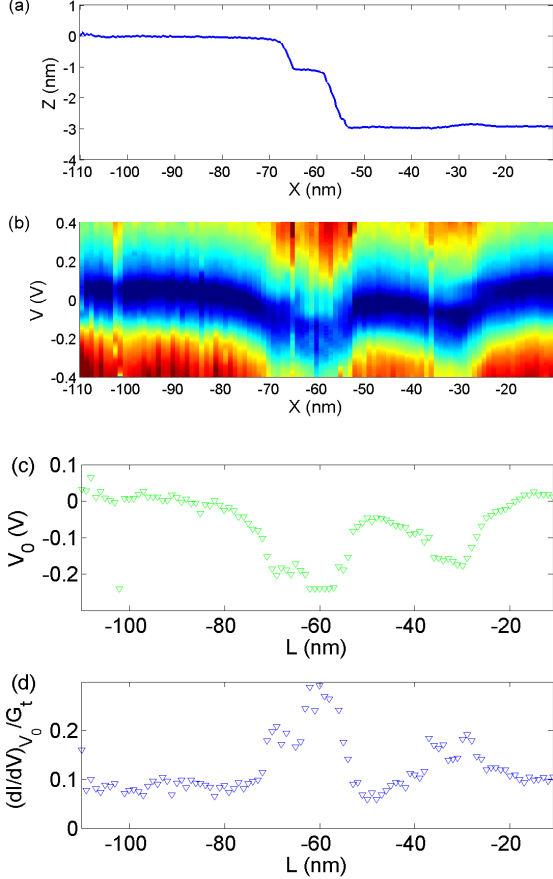


FIG. 4: Profile along a scan line crossing a 1QL and a 2QL step on Bi_2Se_3 (group II) surface (upper curve) and respective set of dI/dV curves (middle, pay attention to the logarithmic color scale) and the Dirac point position along the scan line (bottom). I - V curves were collected at $V_t = -0.4$ V, $I_t = 100$ pA, $T = 5$ K.

due to a finite radius of the tip (≈ 5 nm in this particular case).

Using a set of I - V curves taken in 300 equally separated points along a line (each I - V curve is an average of 20 independent curves taken at the same point) we plot a distribution of the normalized LDOS, $(dI/dV)/G_t$, along the line (Fig. 3(b)). A shift of chemical potential near the step edge is apparent. Namely, the dI/dV curves move as a whole downward by ≈ 0.15 eV while approaching the step and restore their initial position on the lower terrace. A change of the shape of dI/dV curves is also seen.

From the same set of I - V curves we calculate $V_0(L)$ and $dI/dV|_{V=V_0}$ dependences, the results are shown in Fig. 3(c,d). We see that the chemical potential starts to shift at the distance ≈ 10 nm from the step edge Fig. 3(c). The shift corresponds to a positive charge accumulated near the step edge. This shift is accompanied by growth of the differential tunneling conductance at V_0 position

Fig. 3(d).

Very similar features are observed in group II samples. Fig. 4 shows a slice along a horizontal line crossing both 1QL and 2QL steps. Downward shift of dI/dV is also present on the steps as well as on a line defect crossed by the scan line.

STS results on 2D grid

The second type of performed STS measurements is the scanning tunneling spectroscopy on a 2-dimensional grid. It provides much more details about the spatial variation of various physical properties in the vicinity of the step. 100×100 arrays of tunneling spectra of the surfaces shown in Fig. 1 were obtained and used for calculations of V_0 and $dI/dV|_{V=V_0}$ distributions over the surfaces.

Fig. 5(a) and 6(a) visualize distributions of V_0 over the surfaces of Bi_2Se_3 shown in Fig. 1. V_0 exhibits smooth variation within ± 0.05 V along the surface except for the edge step where it decreases by 0.1-0.2 V and reaches its minimum at the step edge. In general, the observed behavior corresponds to that obtained from scans along the lines (Figs. 3 and 4). In addition, macroscopic defects (point and linear defects) are visualized by this method (Fig. 6).

Another data set of our interest is LDOS distribution along the surface. As we are looking for the edge states, it is reasonable to test the spatial distribution of $dI/dV|_{V=V_0}$ which is a measure of LDOS at V_D position. Respective distributions are shown in Fig. 5(b), 6(b). Clearly the edge provokes growth of LDOS within 10 nm region. But this growth does not persist along entire step edge: there are places where growth of LDOS is comparable with LDOS fluctuations (see e.g. the line $y = -87$ nm in Fig. 6(b)).

Let's take a closer look at the tunneling spectra details in the vicinity of steps by using the data obtained upon STS along a line crossing the steps. A reduced set of dI/dV curves from a group I sample illustrating the observed transformations is shown in Fig. 7. On the upper and lower terraces away from the step the curves are as in Fig. 2 with the Dirac cone and a single minimum in the DP. As we move closer to the step edge the curve shifts lower in energy and an increase of tunneling differential conductance occurs in the region of the Dirac point position.

STS data from a line crossing both 1QL and 2QL steps in group II sample demonstrates a more complex behavior (Fig. 8). On the upper and lower terraces away from the steps the curves are as in Fig. 2 with the Dirac cone and a single minimum in the DP. As we move closer to the step edge the curve shifts lower in energy and a region with extra density of states develops around the Dirac point position. Sometimes this development is accompa-

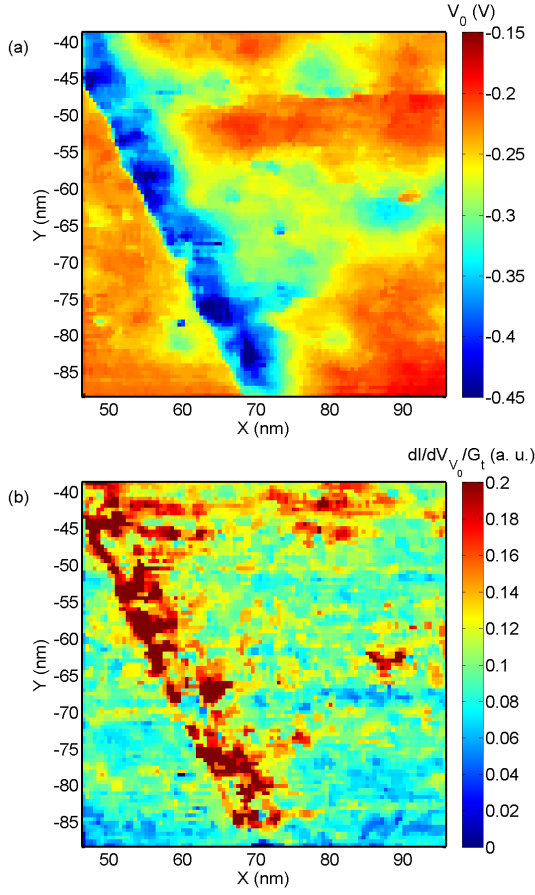


FIG. 5: Distribution of V_0 (a), and $dI/dV|_{V=V_0}$ (b) on Bi_2Se_3 surface shown in Fig. 1(a).

nied by appearance of one or two peaks in LDOS clearly seen in Fig. 8.

DISCUSSION

The most apparent effect is the shift of the chemical potential level, μ , in the vicinity of the step. The shift, $\delta\mu$, has always the same sign, is directed towards the conduction band, varies along a step edge, and depends on the step height. Dependence of $\delta\mu$ vs the step height is shown in Fig. 9 where all the data obtained along individual scan lines are summarized. The correlation between these two quantities is clearly seen. The typical values are $\delta\mu = 100 \pm 50$ meV for 1QL and 150 ± 50 meV for 2QL steps. The data scattering corresponds to the typical level of μ fluctuations far from the edge steps and other macroscopic defects.

A wave function of the surface helical state reach its maximum on a certain depth inside a TI and then decay almost exponentially into a crystal bulk [19, 20]. Analytical expressions for surface state wave function com-

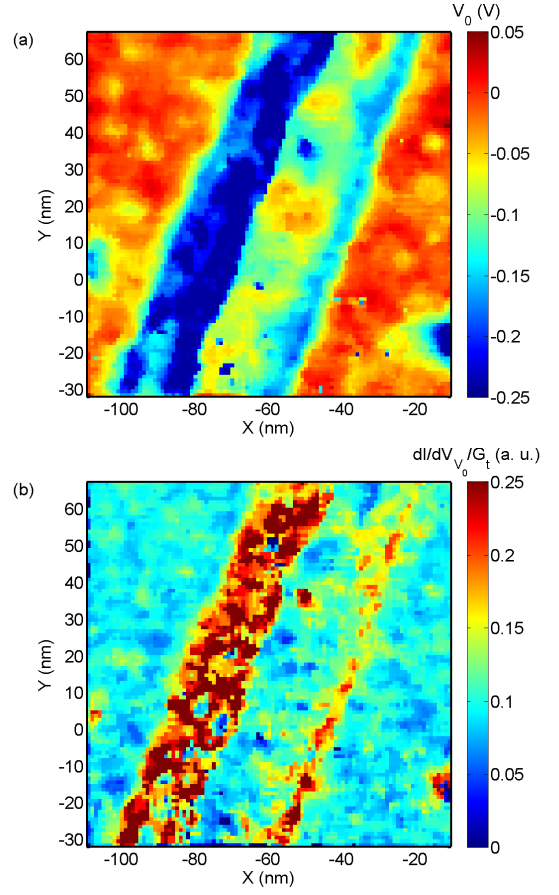


FIG. 6: Distribution of V_0 (a), and $dI/dV|_{V=V_0}$ (b) on Bi_2Se_3 surface shown in Fig. 1(b).

ponents inside the crystal can be written in a form [20]:

$$\Psi = \begin{bmatrix} A_1 \\ A_2 \\ A_3(k_x, k_y) \\ A_4(k_x, k_y) \end{bmatrix} (e^{-\lambda_2 z} - e^{-\lambda_1 z}), \quad (1)$$

where A_i are the wave function components, z is a distance to the surface (from the bulk side), and $\lambda_{1,2}$ are inverse characteristic distances. Fig. 10 shows the envelopes, $e^{-\lambda_2 z} - e^{-\lambda_1 z}$, and $|\Psi|^2$ obtained under various approximations for Bi_2Se_3 [19, 20]. Indeed, in all the cases the surface states are not limited by the first QL: a noticeable fraction extends into the second QL and even the third QL, in agreement with Fig. 9.

Similarly, there is a correlation between the chemical potential shift and its decay length (Fig. 11). We could expect that as the bulk carrier concentration in the groups I is higher than in group II samples, so the characteristic length, l , of the band bending would be shorter. We do not observe such a dependence: l is roughly the same for both groups. We conclude from here that the characteristic length of the band bending is

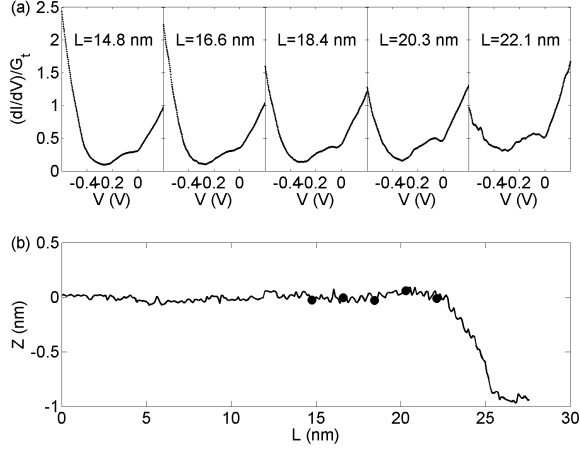


FIG. 7: A set of differential conductance spectra across the 1QL step in Fig. 1 and line profile

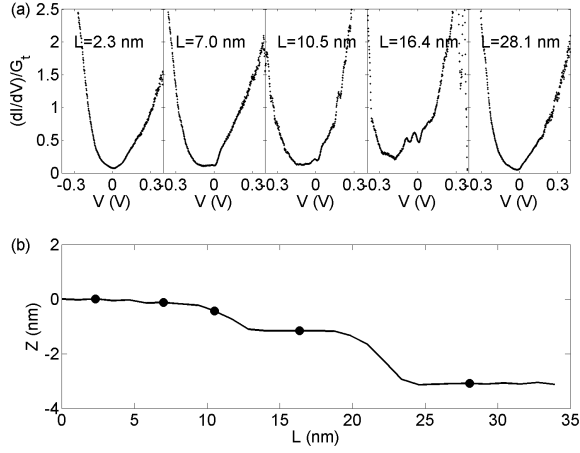


FIG. 8: Profile along a scan line crossing two steps on Bi_2Se_3 (group II) surface (upper curve) and respective set of dI/dV curves (bottom). I - V curves were collected at $V_t = -0.4$ V and $I_t = 100$ pA. $T = 5$ K.

defined mostly by the helical surface states rather than bulk carriers.

Let us consider various contributions to the shift of the chemical level position near the steps. First of all, the observed shift of the chemical potential level towards the bulk conduction bands corresponds to the well known for ordinary metals reduction of the work function near a step edge [17]. The effect results from redistribution of electron wave functions between outer and inner edges of surface steps. We see two quantitative differences in comparison with ordinary metals such as gold [18]: the value of the effect is smaller (0.1 – 0.2 eV instead of 0.9 ± 0.3 eV in gold [18]), but the characteristic length of the effect is bigger (~ 10 nm instead of 0.65 ± 0.01 nm in gold [18]). Such a smaller value of the shift and bigger

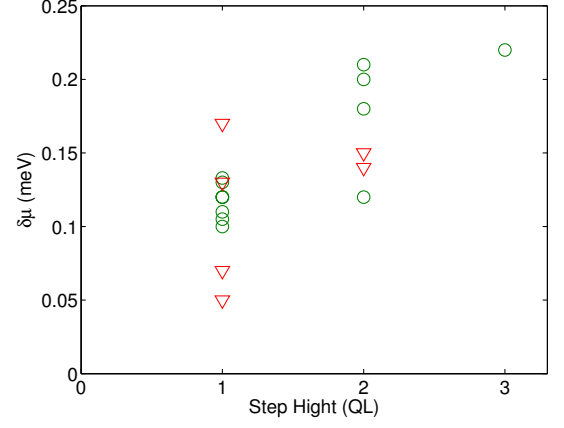


FIG. 9: Correlation between the step height and the chemical potential shift in all studied groups I (circles) and II (triangles) samples.

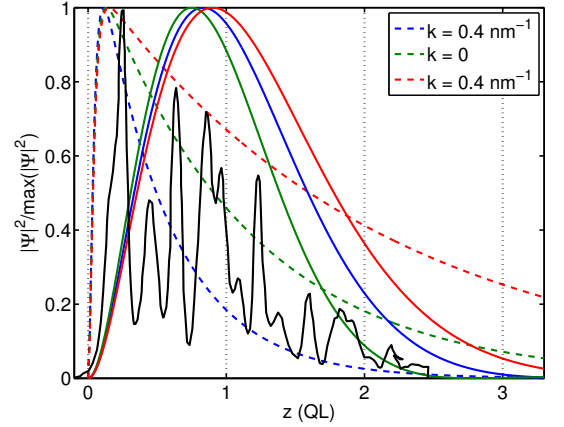


FIG. 10: Wave function amplitudes and envelopes normalized by their maximums in various models. Black solid line: *ab initio* calculations [19]; dashed lines: Eq. (1) with the data of Ref. [20]; color solid lines: Eq. (1) with the data of Ref. [20] extracted from *ab initio* calculations of Ref. [4].

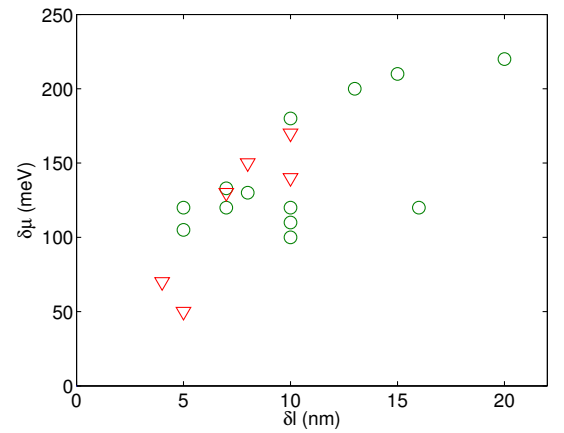


FIG. 11: Correlation between the chemical potential shift and its decay length in all studied groups I (circles) and II (triangles) samples.

length reflects participation of the helical surface states having smaller electron density, n , near the surface ($n \approx \pi k_F^2 / \lambda \sim 3 \times 10^{21} \text{ cm}^{-3}$ for $1/k_F, \lambda \sim 1 \text{ nm}$) than that in usual metals ($n \sim 10^{22} - 10^{23} \text{ cm}^{-3}$). This contribution is considered as a dominating one.

A contribution to this shift may come from the difference of the Dirac point position on different surfaces with respect to the bulk bands. In particular, the position of the Dirac point on (111) surface is 0.15 eV lower than its position at $(\bar{1}10)$ surface [15], so a band bending is expected. In principle, a contribution to the chemical potential shift may also come from a difference of work functions, W , of different surfaces of Bi_2Se_3 coupled electrostatically. The first-principle calculation [15] gives the values of the work function $W_{(111)} = 5.84 \text{ eV}$ and $W_{(\bar{1}10)} = 5.04 \text{ eV}$ for the unrelaxed (111) and $(\bar{1}10)$ surfaces respectively, and 5.81 eV and 4.97 eV for relaxed ones. The sign of the work function change corresponds to our observations.

In addition, a contribution into the chemical potential shift may come from lack of helical surface states near the step edge. Indeed, the topologically protected surface states in Bi_2Se_3 corresponds to relatively small values of the wave vectors, $k \lesssim 0.1 \text{ \AA}^{-1}$. That means lack of the electron concentration in the region $\delta L \sim 1/k$ [9]. In some sense, this contribution is similar to one responsible for reduction of the work function value of stepped surfaces of usual metals [17, 18], but develops inside a crystal. A respective flattening of dI/dV curves in the Dirac point region (see e.g. dI/dV curves in Fig. 7(a) at $L = 18.4 \text{ nm}$ and Fig. 8(a) at $L = 7.0$ and 10.5 nm) may be a signature of this effect.

Comparison of Figs. 5(a) and (b) shows that a noticeable LDOS change at V_0 is observed only in the regions with relatively large change of the chemical potential level $|\delta\mu| \gtrsim 0.1 \text{ eV}$. At higher steps or 1QL step in the vicinity of 2QL step a shift of the chemical potential by $0.15 \pm 0.05 \text{ eV}$ is always present and is accompanied by observable change of LDOS near the step. We also note a correlation between the step height and the LDOS growth. In particular, it is clearly seen from Fig. 8 where the curve at $L = 16.4 \text{ nm}$ demonstrates the biggest extra density, and where all the states on the middle terrace has LDOS higher than any other points on the top and bottom terraces.

In principle, there is a number of possibilities for appearance of extra LDOS in the vicinity of the steps. The most obvious is related to dangling bonds on a side surface. Their overlapping may form an 1D channel along a step. Its fingerprints would be van Hove singularities, as well as possible suppression of states on the Fermi level due to Coulomb interaction [21]. Neither of these contributions is observed. Instead, sometime we observed localized peaks (Fig. 7) which we attribute to localized dangling bonds.

Another possibility was considered by Sen and co-

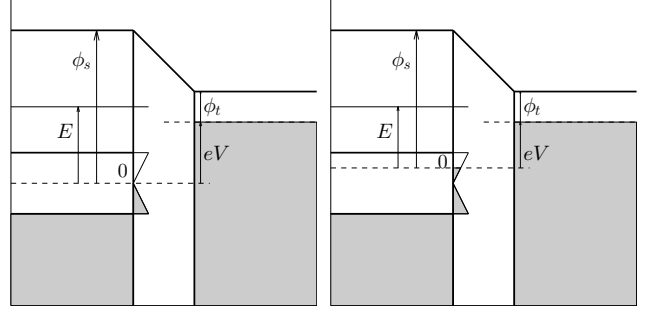


FIG. 12: Energy diagrams for different chemical potential positions. Bulk DOS is omitted for simplicity

authors [10, 13, 14]. They found that the application of a potential barrier along an edge can give rise to states localized at the edge and have a linear energy-momentum dispersion.

But the most serious question is whether the observed growth of $dI/dV|_{V=V_0}$ really corresponds to the increase of LDOS. It will be argued below that a major part (if not all) of the observed $dI/dV|_{V=V_0}$ grows is actually caused by a modification of the transmittance of the vacuum tunneling barrier due to a shift of the chemical potential level.

Let us consider the effect of chemical potential shift, $\delta\mu$, on the tunneling spectra, dI/dV [22]. For our purposes it is enough to analyze the simplest model in zero temperature limit. The tunneling current can be written as

$$I(V) = A \int_0^V \rho_s(E) T(E, V) \rho_t(E - V) dE, \quad (2)$$

where ρ_s and ρ_t are respectively surface and tunneling tip densities of states, and $T(E, V)$ is transmittance of the tunneling gap. In the WKB approximation the transmittance reads

$$T(E, V) = \exp \left(-z \frac{2\sqrt{2m}}{\hbar} \sqrt{\phi + \frac{eV}{2} - E} \right), \quad (3)$$

where z is the tip-sample distance and $\phi = (\phi_s + \phi_t)/2$ is the mean work function of the sample surface and the tip. Shift of the chemical potential modifies both ρ_s and T , the new values are $\bar{\rho}_s(E) = \rho_s(E + \delta\mu)$ and $\bar{T}(E, V) = T(E + \delta\mu/2, V)$ (see Fig. 12). The differential tunneling conductance at the Dirac point, $G = dI/dV|_{V=V_D}$, is then [22]

$$G_D(\mu) = G_D(0) + A \int_0^\mu \rho_s(E) \rho_t \exp \left(-z \frac{2\sqrt{2m}}{\hbar} \sqrt{\phi - E} \right) dE. \quad (4)$$

We see that there is a finite correction to $G_D(0)$. This correction is most noticeable if G_D is small initially, i.e.

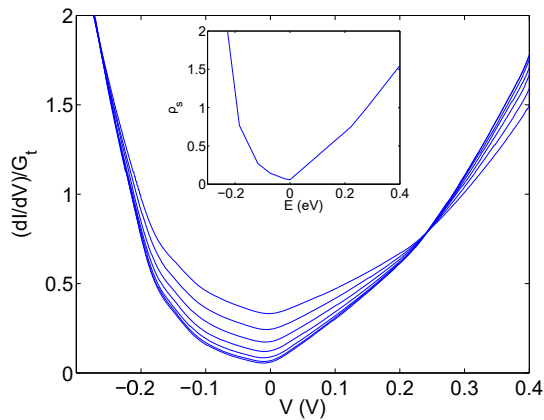


FIG. 13: A set of dI/dV curves obtained in accordance with Eq. 4 for the same energy spectra ρ_s with different positions of the chemical potential level measured from the Dirac point $\mu = 0, 0.05, 0.1, 0.15, 0.2, 0.25, 0.3$ eV, $\phi_s = 5.5$ eV, $z = 1$ nm.

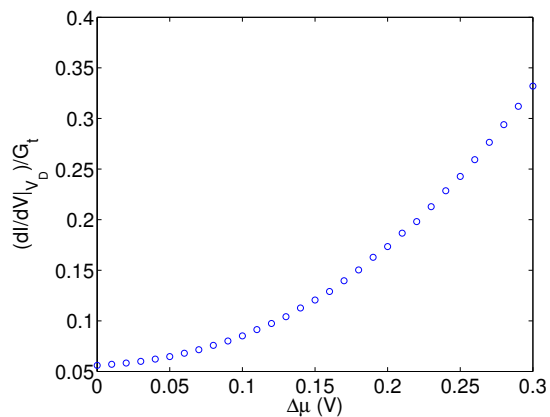


FIG. 14: Effect of chemical potential shift on $dI/dV|_{V=V_0}$ corresponding to the curves shown in Fig. 13.

when $\mu = eV_D$ or very close to this value, as it takes place in the group II samples.

Fig. 13 shows a set of normalized dI/dV curves obtained for the same $\rho_s(E)$ at different values of $\delta\mu$. The curves were obtained for a model $\rho(E)$ (see inset) which produce $I-V$ curves similar to the observed one. We see that the typical shift of the chemical potential by 150 meV produces approximately the same growth of $dI/dV|_{V=V_0}$ by factor 2-3 as it is observed experimentally (Fig. 3(d), 4(d)). Note that similar effect is also present in STS data collected far from defects: normalized $dI/dV|_{V=V_D}$ in group II samples is apparently deeper than that of group I samples (Fig. 2, Fig. 5(b), 6(b) [24]). Similar behavior can be also found in Ref. [23]. As a result, the observed growth of normalized dI/dV near the step edge of the topological insulator Bi_2Se_3 is practically totally accounted by the effect of shift of the chemical potential level. No well reproducible changes of the shape of dI/dV curves near surface steps was found.

We would suggest that p -type thin films of Bi_2Se_3 grown *in situ* and having regular oriented surface steps could be better candidate for experimental search for the edge states.

CONCLUSION

We demonstrate here that the energy structure of the surface states of the topological insulator Bi_2Se_3 revealed by STS exhibits dramatic changes near the step edge: there is shift of the chemical potential level which is accompanied by apparent growth of dI/dV value at the Dirac point. Various contributions into the chemical potential shift are analyzed. The most universal one corresponds qualitatively to reduction of the work function on stepped surfaces of topologically trivial (normal) metals. Quantitative differences (smaller value of the chemical potential shift and bigger spatial scale) reflect specifics of topological insulators: smaller surface current carrier concentration and smaller wave vectors of the surface helical states. We also demonstrate here that the apparent growth of dI/dV is actually the artifact of the STS method. This growth is almost entirely accounted by the voltage-dependent transparency of the tunneling barrier and therefore cannot be considered as an indication of increase of LDOS near the step edge.

We are grateful to V.A. Sablikov and V.V. Pavlovskii for useful discussions and V.F. Nasretdinova for help in crystal growth. Financial supports from RSF (project # 16-12-10335, experimental part) and RFBR (project #16-02-00677, effect of the chemical potential) are acknowledged.

-
- [1] I. Tamm, Phys. Z. Soviet Union 1: 733 (1932).
 - [2] W. Shockley, Phys. Rev. **59**, 319 (1939).
 - [3] As a review see: Topological Insulators: Fundamentals and Perspectives, Eds.: Frank Ortmann, Stephan Roche, Sergio O. Valenzuela, Laurens W. Molenkamp, Wiley (2015); Contemporary Concepts of Condensed Matter Science, Eds.: E.Burstein, A.H. Macdonald and P. J. Stiles, Vol. 6, Topological Insulators, Eds.: M. Franz, L. Molenkamp, Elsevier, Oxford, 2013.
 - [4] H. Zhang, Ch.-X. Liu, X.-L. Qi, X. D., Zh. Fang and Sh.-Ch. Zhang, Nature Phys. **5** 438 (2009).
 - [5] L. Simon, C. Bena, F. Vonau, M. Cranney and D. Auel, Journal of Physics D: Applied Physics, **44**, 464010 (2011).
 - [6] T. Zhang, P. Cheng, X. Chen, J. F. Jia, X. Ma, K. He, L. Wang, H. Zhang, X. Dai, Z. Fang, X. Xie, and Q. K. Xue, Phys. Rev. Lett., **103**, 266803 (2009).
 - [7] Zh. Alpichshev, J. G. Analytis, J.-H. Chu, I. R. Fisher, and A. Kapitulnik, Phys. Rev. B **84**, 041104(R) (2011).
 - [8] C.-L. Song, L. Wang, K. He, S.-H. Ji, X. Chen, X.-C. Ma, and Q.-K. Xue, Phys. Rev. Lett. **114**, 176602 (2015).

- [9] R.R. Biswas and A.V. Balatsky, Phys. Rev. B **83**, 075439 (2011).
- [10] D. Sen and O. Deb, Phys. Rev. B **85**, 245402 (2012).
- [11] Y. Takane and Ken-Ichiro Imura, J. Phys. Soc. Jpn. **81**, 093705 (2012).
- [12] T. Paananen and Th. Dahm, Phys. Rev. B **87**, 195447 (2013).
- [13] R. Seshadri and D. Sen, Phys. Rev. B **89**, 235415 (2014).
- [14] O. Deb, A. Soori and D. Sen, J. Phys.: Condens. Matter **26**, 315009 (2014).
- [15] Y.-L. Lee, H. Ch. Park, J. Ihm, and Y.-W. Son, PNAS, **112**, 11514 (2015).
- [16] A.Yu. Dmitriev, N.I. Fedotov, V.F. Nasretdinova, S.V. Zaitsev-Zotov, JETP Letters, **100**, 398 (2014).
- [17] R. Smoluchowski, Phys. Rev. **60**, 661 (1941).
- [18] J.F. Jia, K. Inoue, Y. Hasegawa, W.S. Yang, T. Sakurai, Phys. Rev. B **58**, 1193 (1998).
- [19] S.V. Eremeev, M.G. Vergniory, T.V. Menshchikova, A.A. Shaposhnikov and E.V. Chulkov, New Journal of Physics **14**, 113030 (2012).
- [20] Wen-Yu Shan, Hai-Zhou Lu and Shun-Qing Shen, New Journal of Physics **12**, 043048 (2010).
- [21] J. Voit, Rept. Prog. Phys., **58**, 977 (1995).
- [22] N.I. Fedotov, S.V. Zaitsev-Zotov, to be published in JETP Letters; arXiv:1609.08294.
- [23] J. Dai, D. West, X. Wang, Y. Wang, D. Kwok, S.-W. Cheong, S.B. Zhang, and W. Wu, Phys. Rev. Lett. **117**, 106401 (2016).
- [24] Bear in mind the difference in normalization of dI/dV curves of groups I and II samples.